

A Hierarchical Control Framework for Drift Maneuvering of Autonomous Vehicles

Bo Yang, Yiwen Lu, Xu Yang and Yilin Mo¹

Abstract—Drift control is significant to the safety of autonomous vehicles when there is a sudden loss of traction due to external conditions such as rain or snow. It is a challenging control problem due to the presence of significant sideslip and nearly full saturation of the tires. In this paper, we focus on the control of drift maneuvers following circular paths with either fixed or moving centers, subject to change in the tire-ground interaction, which are common training tasks for drift enthusiasts and can therefore be used as benchmarks of the performance of drift control. In order to achieve the above tasks, we propose a novel hierarchical control architecture which decouples the curvature and center control of the trajectory. In particular, an outer loop stabilizes the center by tuning the target curvature, and an inner loop tracks the curvature using a feedforward/feedback controller enhanced by an \mathcal{L}_1 adaptive component. The hierarchical architecture is flexible because the inner loop is task-agnostic and adaptive to changes in tire-road interaction, which allows the outer loop to be designed independent of low-level dynamics, opening up the possibility of incorporating sophisticated planning algorithms. We implement our control strategy on a simulation platform as well as on a 1/10 scale Radio-Control (RC) car, and both the simulation and experiment results illustrate the effectiveness of our strategy in achieving the above described set of drift maneuvering tasks.

I. INTRODUCTION

In recent years, autonomous driving has drawn increasing attention in academia and industry [1], with subareas including but not limited to environment perception [2]–[4], motion planning [5]–[7] and motion control [8]–[10]. In this paper, we focus on drift control, an extreme instance of motion control where significant slip exists between the tires and the ground [11]. Drift control is pertinent to the safety of autonomous driving because significant slip may occur unexpectedly due to external conditions like rain or snow and cause a sudden loss of traction, where the precise control of the vehicle trajectory is required to avoid accidents. More specifically, we focus on *drift maneuvering*, which involves manipulating the vehicle to track certain trajectories in sustained drift [11], and can therefore be viewed as a benchmark of drift control performance.

Drift maneuvering is challenging due to tire saturation and limited control authority in a highly unstable region [11]. As a result, it is usually tackled on a per-task or per-vehicle basis in the existing literature. For example, Goh et

al. [12] reformulate a fixed circular trajectory as a series of vehicle-dependent drift equilibrium points, based on which they propose tracking controllers for the sideslip error and lookahead error, and Goh et al. [13] extend the above work to tracking arbitrary pre-defined trajectories by casting the vehicle dynamics into a trajectory-dependent curvilinear coordinate system, in which they apply nonlinear model inversion to minimize the tracking error. Both the two works, however, are mechanism-based methods that rely on accurate modeling of the vehicle dynamics and parameterization of the reference trajectory, a process that can be tedious if the methods are to be deployed to different vehicles and applied to perform generic drift maneuvering tasks. Culter et al. [14], on the contrary, adopt the data-driven approach to drift maneuvering by applying an reinforcement learning algorithm called Probability Inference for Learning COntrol (PILCO), but the method is only considered in a single-task setting, where the objective is to minimize tracking error of a particular drift equilibrium. Like other reinforcement learning algorithms [15], ad hoc reward shaping and a significant amount of training data may be required for the method to generalize across different drift maneuvering tasks. Apart from the mechanism-based and data-driven methods, another class of drift maneuvering methods are aided by expert experience, including Jelavic et al. [16] and Zhang et al. [11], [17], which apply either a feedforward/feedback controller or an open-loop controller to track an expert trajectory in some phase of the drifting process. A drawback of the expert-aided methods is that human experience has limited coverage of different drifting conditions, and as a result, those methods are usually designed to track a particular trajectory. Moreover, none of the above works consider the sudden change of tire-ground interaction, a practical situation that may occur due to external conditions like rain or snow.

In this paper, we propose a novel drift control framework that can perform various maneuvering tasks and adapt to sudden changes of tire-ground interaction. The flexibility of our framework stems from the observation that a generic drift trajectory can be viewed as an arc with continuously varying center and curvature, based on which we propose a hierarchical architecture that decouples the center and curvature control of the trajectory. In particular, an outer loop stabilizes the center by tuning the target curvature, and an inner loop tracks the curvature using a feedforward/feedback controller enhanced by an \mathcal{L}_1 adaptive control [18] component. Through an adaptive feedforward and reference signal design, the inner loop can deliver a consistent curvature tracking performance over different tire-ground interaction,

*This work is supported by the National Key Research and Development Program of China under Grant 2018AAA0101601

¹The authors are with Department of Automation and BNRist, Tsinghua University, Beijing, China {yang-b21, luyw20, yangx21}@mails.tsinghua.edu.cn, ylmo@tsinghua.edu.cn

allowing the outer loop to focus on maneuver navigation, such that it can achieve various tasks without knowing the internal details of the vehicle dynamics.

A key contribution of our control architecture described above is the introduction of *curvature feedback*, which serves as a bridge between the low-level vehicle stabilization and the high-level navigation. In contrast to the aforementioned previous works that are built upon state feedback, our proposed controller makes decisions based on both the vehicle state and the trajectory curvature. The reason for this design is we identify that curvature, as a quantity decided by a sequence of states over a time window, encodes higher-level information about the maneuver trajectory than a single state, while still maintaining the ease of control by a straightforward inner-loop structure.

In this paper, we illustrate the effectiveness of our control strategy on the drift maneuver on a circular path with either fixed or moving center, subject to changes in the tire-ground interaction, which are common training tasks for drifting enthusiasts [19]. We also believe our proposed hierarchical control architecture can potentially incorporate more sophisticated planning algorithms, e.g., the one proposed by Levin et al. [20], which plans trajectories by concatenating motion primitives. The belief is based on the identification that a motion primitive for drifting can be represented in terms of a sequence of curvature values, and such sequences, common in the aforementioned drift training tasks, have been shown to be accurately tracked by our proposed controller in both simulation and hardware experiments.

II. PROBLEM FORMULATION

For controller design and simulation, we abstract the vehicle into a bicycle model with side slip. On one hand, we ignore the difference between left and right wheels, which is usually insignificant in drift maneuvering [11]. On the other hand, for a relatively high-fidelity characterization of the tire slip, which is an essential feature of drift, we model the tire-ground interaction using the famous Pacejka Magic Formula [21]. The above mixed-fidelity vehicle modeling for aggressive maneuvering has been reported and proved effective in [22], [23]. An illustration of the model is given in Fig. 1.

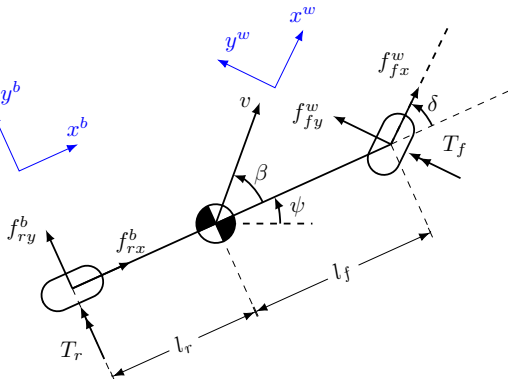


Fig. 1: Illustration of car model

We assume the vehicle is four-wheel driven, and that all its wheels have the same rotational speed specified as an input. Correspondingly, the state and input vectors are

$$\mathbf{X} = [x, y, \psi, \dot{x}, \dot{y}, \dot{\psi}]^T, \mathbf{U} = [\delta, \omega]^T, \quad (1)$$

where x, y are the coordinate of the vehicle in a two-dimensional plane, ψ is the heading angle, $\dot{x}, \dot{y}, \dot{\psi}$ are the time derivatives of x, y, ψ ; δ is the front wheel steering angle, and ω is the rotational speed of the wheels. The dynamic equations are

$$m\ddot{x} = f_{fx}^w \cos(\psi + \delta) - f_{fy}^w \sin(\psi + \delta) + f_{rx}^b \cos \psi - f_{ry}^b \sin \psi, \quad (2)$$

$$m\ddot{y} = f_{fx}^w \sin(\psi + \delta) + f_{fy}^w \cos(\psi + \delta) + f_{rx}^b \sin \psi + f_{ry}^b \cos \psi, \quad (3)$$

$$I_z \ddot{\psi} = (f_{fy}^w \cos \delta + f_{fx}^w \sin \delta) l_f - f_{ry}^b l_r, \quad (4)$$

where m is the mass of the vehicle, I_z is the moment of inertia of the vehicle body w.r.t. the z axis, r_f, r_r are the radii of the wheels, l_f, l_r are the distances of the wheels to the center of mass of the vehicle, and $f_{fx}^w, f_{fy}^w, f_{rx}^b, f_{ry}^b$ are the friction forces. The subscripts ‘f’, ‘r’ refer to “front” and “rear” respectively, and the superscripts ‘w’ and ‘b’ refer to “front wheel frame” and “body frame” respectively. We make the distinction between the ‘w’ and ‘b’ frames due to the existence of the front wheel steering angle. The friction forces are determined by

$$f_{fx}^w = \mu_{fx} f_{fz}, f_{fy}^w = \mu_{fy} f_{fz}, f_{rx}^b = \mu_{rx} f_{rz}, f_{ry}^b = \mu_{ry} f_{rz},$$

where $\mu_{fx}, \mu_{fy}, \mu_{rx}, \mu_{ry}$ are the friction coefficients, and f_{fz}, f_{rz} are the normal forces. The friction coefficients are described by

$$\mu_{ij} = -\frac{s_{ij}}{s_i} D \sin(C \arctan(B s_i)) \quad (i \in \{f, r\}, j \in \{x, y\}), \quad (5)$$

where B, C, D are parameters that vary with the tyre-ground interaction properties, and s_i, s_{ij} are slip ratios that can be computed from relative speeds between the wheels and the road:

$$s_i = \sqrt{s_{ix}^2 + s_{iy}^2}, \quad (i \in \{f, r\}), \quad (6)$$

$$s_{fx} = \frac{v_{fx}^w - \omega r_f}{\omega r_f}, s_{fy} = \frac{v_{fy}^w}{\omega r_f}, \quad (7)$$

$$s_{rx} = \frac{v_{rx}^b - \omega r_r}{\omega r_r}, s_{ry} = \frac{v_{ry}^b}{\omega r_r}, \quad (8)$$

$$v = \sqrt{\dot{x}^2 + \dot{y}^2}, \beta = \arctan \frac{\dot{y}}{\dot{x}} - \psi, \quad (9)$$

$$v_{fx}^w = v \cos(\beta - \delta) + \dot{\psi} l_f \sin \delta, v_{rx}^b = v \cos \beta, \quad (10)$$

$$v_{fy}^w = v \sin(\beta - \delta) + \dot{\psi} l_f \cos \delta, v_{ry}^b = v \sin \beta - \dot{\psi} l_r. \quad (11)$$

Finally, the normal forces f_{fz}, f_{rz} can be determined as:

$$f_{fz} = \frac{l_r - \mu_{rx} h}{l_f + l_r + (\mu_{fx} \cos \delta - \mu_{fy} \sin \delta - \mu_{rx}) h} mg, \\ f_{rz} = \frac{l_f + (\mu_{fx} \cos \delta - \mu_{fy} \sin \delta) h}{l_f + l_r + (\mu_{fx} \cos \delta - \mu_{fy} \sin \delta - \mu_{rx}) h} mg.$$

The goal of our controller is driving the vehicle to perform various maneuvers while maintaining it in the drift condition, characterized by a nontrivial sideslip angle β (defined in (9)) [11], e.g., $\beta = -\pi/3$ during a counter-clockwise move. To illustrate, a vehicle performing a drift maneuver is sketched in Fig. 2. In particular, we consider the following drift maneuver tasks in this paper because they are common training tasks for drift enthusiasts and can therefore be used as benchmarks of the capability of drift control:

- **Fixed-circle drifting:** tracking a circle path with fixed center and radius while drifting.
- **Varying-center drifting:** drifting in a circular manner, with the desired center moving.
- **Varying-interaction drifting:** drifting across ground textures with different tyre-ground interaction parameters B, C, D (c.f. (5)).

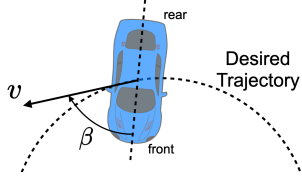


Fig. 2: Illustration of vehicle performing a drift maneuver

III. CONTROL ARCHITECTURE

An overview of our control architecture is presented in Fig. 3. Our controller consists of three components: i) state, curvature and friction estimators, which provide both low- and high-level descriptions of the current drifting situation; ii) an inner-loop feedforward/feedback controller, which aims to track target curvature κ_{ref} while maintaining the vehicle in sustained drift; iii) an outer-loop controller for center stabilization, which decides a feasible curvature for the inner-loop controller to track, according to the expected center and radius $C_{\text{exp}}, R_{\text{exp}}$ provided by the task specification. A main feature of our control architecture is the estimation of and feedback on the curvature κ , a key quantity that allows us to decouple of the inner and outer loops, which are responsible for the low-level vehicle stabilization and high-level task completion responsively. In addition, besides the standard state estimator and feedback controller blocks, we adopt a friction estimator for tuning the feedforward signals according to the perceived tyre-ground interaction parameters, and an \mathcal{L}_1 Adaptive Control ($\mathcal{L}_1\text{AC}$) module for optimizing the transient characteristics of the inner loop, both of which serve to improve the adaptive performance of our controller. For the rest of this section, we describe each of the three components of our control architecture in detail.

A. Estimators

For state estimation, we adopt the Kalman Filter (KF) to fuse position and angular velocity measurements from both on-board sensors, e.g., Inertial Measurement Unit (IMU), and off-board sensors, e.g., the motion capture system. Taking communication delay into account, we implement the KF in

an asynchronous manner [24], performing an update upon the arrival of each new observation from any sensor.

For both curvature and friction estimation, we utilize state and input data (defined in (1)) from a recent time window of T steps, denoted by $\{\mathbf{X}^{(i)}, \mathbf{U}^{(i)}\}_{i=-T+1}^0$.

For curvature estimation, we fit a circle centered at (x_0, y_0) with radius R that approximately crosses those T points, by solving the following nonlinear optimization problem:

$$\begin{aligned} \arg \min_{x_0, y_0, R} & \sum_{i=1}^T \left(R_{\text{geo}}^{(i)} - R^2 \right)^2 + \left(R_{\text{kin}}^{(i)} - R^2 \right)^2, \\ \text{s.t. } R_{\text{geo}}^{(i)} &= \sqrt{(x^{(i)} - x_0)^2 + (y^{(i)} - y_0)^2}, \\ R_{\text{kin}}^{(i)} &= \frac{\sqrt{(\dot{x}^{(i)})^2 + (\dot{y}^{(i)})^2}}{|\dot{\psi}^{(i)}|}, \\ R &= \sum_{i=1}^T \frac{R_{\text{geo}}^{(i)} + R_{\text{kin}}^{(i)}}{2}, \end{aligned}$$

and obtain the curvature κ according to $\kappa = R^{-1}$. In contrast to existing geometry-based circle estimators [25], our algorithm complements geometric information with kinematics information (denoted by R_{geo} and R_{kin} respectively in the above formulation), which leverages the full power of position and angular velocity sensors.

For friction estimation, we assume a constant friction coefficient $\mu(B, C, D) = D \sin(C \arctan(Bs_f)) = D \sin(C \arctan(Bs_r))$ during drift (c.f. (5)) for each set of tyre-ground interaction parameter (B, C, D) , which agrees with our empirical observations. Based on this assumption, the friction estimator attempts to find μ that best explains the observed data by solving the following optimization problem:

$$\min_{\mu} \sum_{i=-T+1}^0 \ell \left(f(\mathbf{X}^{(i)}, \mathbf{U}^{(i)}; \mu), \mathbf{X}^{(i+1)} \right),$$

where ℓ denotes the ℓ_2 loss, f denotes the discretized dynamics equations (2)-(5) with $D \sin(C \arctan(Bs_i))$ replace by μ . Once the estimated friction coefficient μ is obtained, the corresponding optimal feedforward control inputs $\delta_{\text{ff}}, \omega_{\text{ff}}$ can be found by looking up a table of drift equilibria collected offline.

B. Inner-loop Controller

The basis of our inner-loop controller is two PID feedback control loops, one of which controls the sideslip angle β by tuning the front wheel steering angle δ , and the other of which controls the curvature κ by tuning the wheel rotational speed ω . Feedforward signals $\delta_{\text{ff}}, \omega_{\text{ff}}$, which depend on tyre-ground friction coefficient μ (see subsection III-A) and target curvature, are supplemented to the feedback controller to speed up the transient process.

We applied \mathcal{L}_1 adaptive output feedback controller proposed by Cao et al. [26] to optimize the transient performance of radius response. The structure of \mathcal{L}_1 adaptive output feedback controller is shown in the Figure 4. $A(s)$ represents the vehicle dynamic system with feedforward and

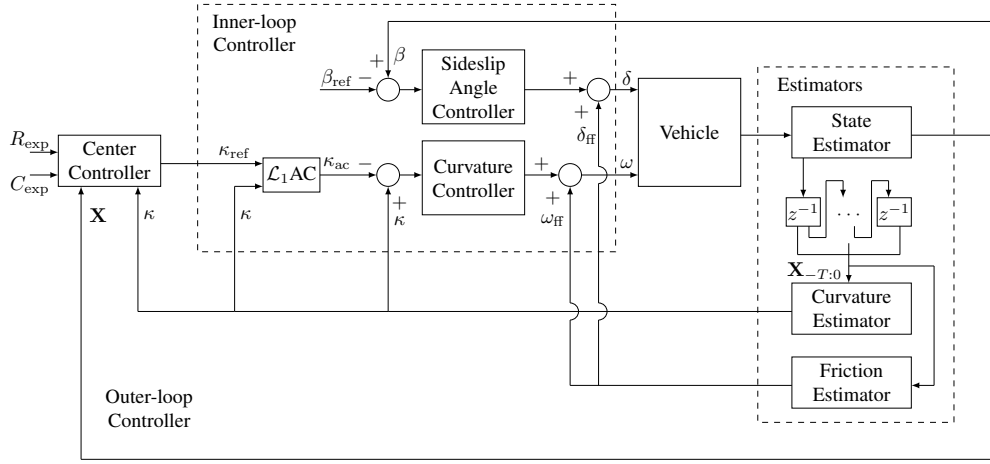


Fig. 3: Overview of our control architecture

feedback controller, which is so complex that difficult to accurately model. $d(s)$ means the disturbance comes from changes in the tyre-ground interaction characteristics and failure of the actuators. τ describes the communication delay of the ROS network, which is an important factor that affects the performance of the controller. r is the reference curvature input. $M(s)$ is the desired reference model with excellent radius response properties. $C(s)$ is the low-pass filter, which limits the bandwidth of radius control signal to avoid high frequency oscillation while maintaining a fast adaptive rate. The most important advantage of \mathcal{L}_1 adaptive control is the decoupling of control loop and the estimation loop, so that both transient performance and robustness can be guaranteed.

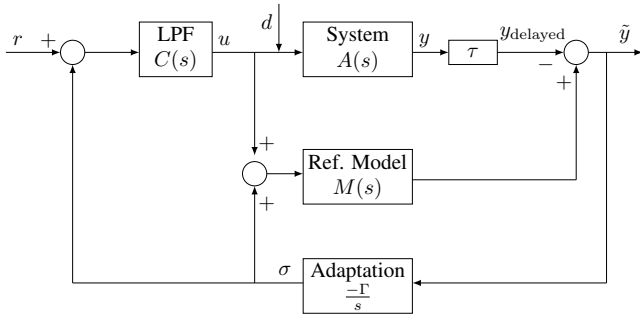


Fig. 4: \mathcal{L}_1 output feedback adaptive control [18]

Hindman et al. [27] analyze \mathcal{L}_1 adaptive output feedback control in detail and then give the specific expression of the closed-loop response: $y(s) = H(s)C(s)r(s) + H(s)(1 - C(s))d(s)$, where $H(s) = \frac{A(s)M(s)}{C(s)A(s) + (1 - C(s))M(s)}$.

By designing the reference model $M(s)$ and the low-pass filter $C(s)$ and the adaptive gain Γ , the ideal closed-loop response $H(s)C(s)$ with respect to the radius R can be obtained. Michini et al. [18] provided a design method of \mathcal{L}_1 output feedback adaptive controller.

IV. SIMULATION AND EXPERIMENT

A. Simulation Results

To demonstrate the effectiveness of our control strategy, three drift maneuver tasks mentioned above are implemented on the simulation platform.

The first task is fixed-circle drifting, where the expected center is (0,0) and the expected radius is 10m.

In this task, we analyze the process of starting drift, which involves a huge state transition and complex dynamics. In many of the previous works on drift maneuver control, open-loop commands based on expert experience are required to get the vehicle close to the unstable drift equilibrium points. By contrast, the proposed controller can complete the process of starting drift successfully without any expert experience, which can be noticed in Fig. 5. As shown in Fig. 5, the rise time of β , which represents the speed of starting drift, is about 2 seconds, while the adjustment time β , which represents the speed of stabilizing drift, is about 10 seconds. These characteristics show that our controller makes the vehicle quickly reach the steady drift state. As shown in Fig. 5, in the phase of starting drift, the actual R does not accurately track the reference R , but the actual R is always around the target $R(=10\text{m})$ with a deviation of $\leq 3\text{m}$, which makes the trajectory not deviate too much from the target circle. It can also be observed from the Fig. 5 and Fig. 5 that there is no steady-state error of β and R .

The second task is varying-center drifting, where the expected center is also making a circular motion with (0,0) as the center and 15m as the radius.

In this task, we analyze the tracking of the moving center in steady drift state, which requires quickly adjust drift equilibrium to achieve real-time tracking. As shown in Fig. 5, the trajectory of the actual center is smooth and fits the trajectory of the desired center, which demonstrates that by adopting hierarchical structure in the proposed controller, the center and the radius can be decoupled and accurately controlled. Comparing Fig. 5 and Fig. 6, the phenomenon that β remains almost unchanged while R periodically changes can be observed, which verifies that by using controllers with

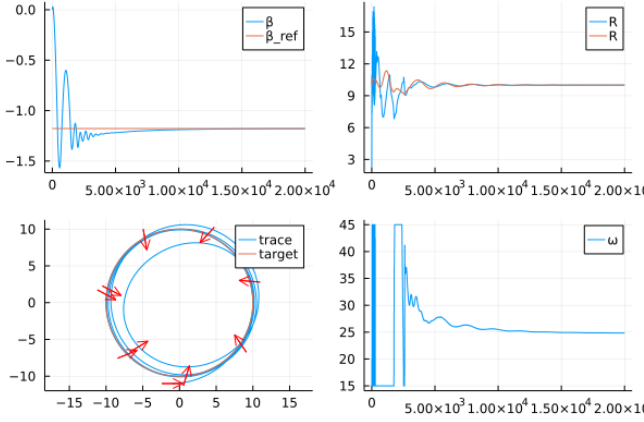


Fig. 5: Fixed-circle drifting

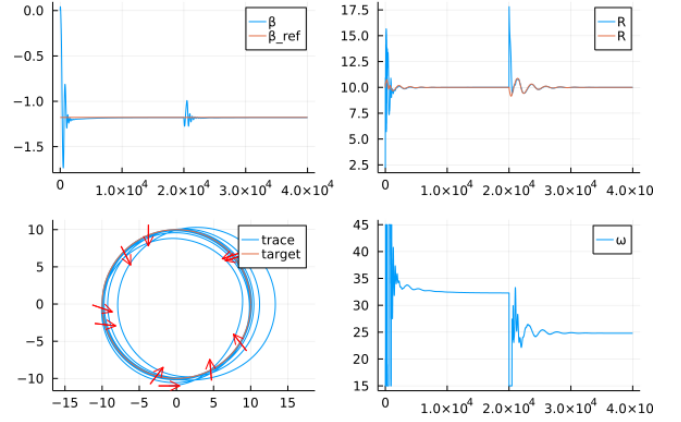


Fig. 7: Vary-texture drifting

different frequencies for β and R , the decoupling of β and R can be achieved while maintaining high control accuracy.

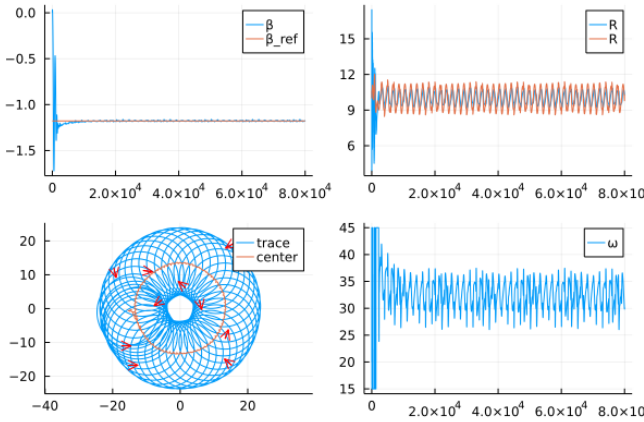


Fig. 6: Move-center drifting

The third task is varying-interaction drifting, where time varying ground friction coefficient is introduced into the simulation. The coefficient of friction before the change is $\mu=0.121$, while the coefficient of friction after the change is $\mu=0.074$, and the moment of change is at $t=150s$. The comparison shows that the friction coefficient has a very large change, which is a huge challenge for the robustness of the controller. Firstly, Fig. 5 shows that although there is a large change in friction coefficient, the maximum deviation of the trajectory from the reference trajectory is only 3.5m, moreover, this deviation is quickly adjusted to around 0m. As shown in Fig. 5 and Fig. 6, when the friction coefficient changes suddenly, both β and R change rapidly, especially R has a significant rise. However, the proposed controller has strong adaptive ability and robustness, which enables it to quickly response to sudden changes in friction coefficient, therefore, both β and R can be quickly stabilized to the reference value.

B. Experiment Results

The RC car used for the hardware experiments is shown in Fig. 8, In order to complete the curvature estimation, we implement asynchronous Kalman filter [24] to fuse the data from motion capture system and IMU. The proposed hierarchical controller is lightweight and efficient, allowing it to run on-board at a high frequency of 100Hz. All these drift maneuver experiments are available in: [url](#)



Fig. 8: RC car used in the experiments, equipped with NVIDIA Jetson TX2, IMU, Motion capture system fluorescent balls, Hokuyo UST-10LX Lidar, Stereo ZED Camera

V. CONCLUSION

This works developed a controller with hierarchical architecture for the drift maneuver control of autonomous vehicles. In the proposed controller, curvature feedback is introduced to decouple the center and curvature into inner and outer loop: the outer loop stabilizes the center, while the inner loop tracks the curvature. In order to respond quickly and accurately to curvature changes in complex tasks and environments, a feedforward/feedback controller enhanced by \mathcal{L}_1 adaptive component is adopted in the inner loop to increase the robustness of the controller. Experimental Results demonstrate that the proposed controller can achieve high performance drift maneuver control. The future work is to integrate high-level curvature-based path planners to achieve drift maneuver control of arbitrary trajectories.

REFERENCES

- [1] B. Paden, M. Cap, S. Z. Yong, D. Yershov, and E. Frazzoli, "A survey of motion planning and control techniques for self-driving urban vehicles," 2016.
- [2] J. Janai, F. Güney, A. Behl, A. Geiger, *et al.*, "Computer vision for autonomous vehicles: Problems, datasets and state of the art," *Foundations and Trends® in Computer Graphics and Vision*, vol. 12, no. 1–3, pp. 1–308, 2020.
- [3] Y. Wang, W.-L. Chao, D. Garg, B. Hariharan, M. Campbell, and K. Q. Weinberger, "Pseudo-lidar from visual depth estimation: Bridging the gap in 3d object detection for autonomous driving," in *Proceedings of the IEEE/CVF Conference on Computer Vision and Pattern Recognition*, pp. 8445–8453, 2019.
- [4] P. Sun, H. Kretzschmar, X. Dotiwalla, A. Chouard, V. Patnaik, P. Tsui, J. Guo, Y. Zhou, Y. Chai, B. Caine, *et al.*, "Scalability in perception for autonomous driving: Waymo open dataset," in *Proceedings of the IEEE/CVF Conference on Computer Vision and Pattern Recognition*, pp. 2446–2454, 2020.
- [5] M. McNaughton, C. Urmson, J. M. Dolan, and J.-W. Lee, "Motion planning for autonomous driving with a conformal spatiotemporal lattice," in *2011 IEEE International Conference on Robotics and Automation*, pp. 4889–4895, IEEE, 2011.
- [6] J. Wei, J. M. Snider, T. Gu, J. M. Dolan, and B. Litkouhi, "A behavioral planning framework for autonomous driving," in *2014 IEEE Intelligent Vehicles Symposium Proceedings*, pp. 458–464, IEEE, 2014.
- [7] D. Dolgov, S. Thrun, M. Montemerlo, and J. Diebel, "Practical search techniques in path planning for autonomous driving," *Ann Arbor*, vol. 1001, no. 48105, pp. 18–80, 2008.
- [8] M. Elbanhawi, M. Simic, and R. Jazar, "Receding horizon lateral vehicle control for pure pursuit path tracking," *Journal of Vibration and Control*, vol. 24, no. 3, pp. 619–642, 2018.
- [9] L. Ni, A. Gupta, P. Falcone, and L. Johansson, "Vehicle lateral motion control with performance and safety guarantees," *IFAC-PapersOnLine*, vol. 49, no. 11, pp. 285–290, 2016.
- [10] L. Zhang, Y. Wang, and Z. Wang, "Robust lateral motion control for in-wheel-motor-drive electric vehicles with network induced delays," *IEEE Transactions on Vehicular Technology*, vol. 68, no. 11, pp. 10585–10593, 2019.
- [11] F. Zhang, J. Gonzales, S. E. Li, F. Borrelli, and K. Li, "Drift control for cornering maneuver of autonomous vehicles," *Mechatronics*, vol. 54, pp. 167–174, 2018.
- [12] J. Y. Goh and J. C. Gerdes, "Simultaneous stabilization and tracking of basic automobile drifting trajectories," in *2016 IEEE Intelligent Vehicles Symposium (IV)*, pp. 597–602, IEEE, 2016.
- [13] J. Y. Goh, T. Goel, and J. Christian Gerdes, "Toward automated vehicle control beyond the stability limits: drifting along a general path," *Journal of Dynamic Systems, Measurement, and Control*, vol. 142, no. 2, p. 021004, 2020.
- [14] M. Cutler and J. P. How, "Autonomous drifting using simulation-aided reinforcement learning," in *2016 IEEE International Conference on Robotics and Automation (ICRA)*, pp. 5442–5448, IEEE, 2016.
- [15] G. Dulac-Arnold, N. Levine, D. J. Mankowitz, J. Li, C. Paduraru, S. Goyal, and T. Hester, "Challenges of real-world reinforcement learning: definitions, benchmarks and analysis," *Machine Learning*, pp. 1–50, 2021.
- [16] E. Jelavic, J. Gonzales, and F. Borrelli, "Autonomous drift parking using a switched control strategy with onboard sensors," *IFAC-PapersOnLine*, vol. 50, pp. 3714–3719, 2017.
- [17] F. Zhang, J. Gonzales, K. Li, and F. Borrelli, "Autonomous drift cornering with mixed open-loop and closed-loop control," *IFAC-PapersOnLine*, vol. 50, no. 1, pp. 1916–1922, 2017. 20th IFAC World Congress.
- [18] B. Michini and J. How, "L1 adaptive control for indoor autonomous vehicles: Design process and flight testing," in *AIAA Guidance, Navigation, and Control Conference*, p. 5754, 2009.
- [19] M. Abdulrahim, "On the dynamics of automobile drifting," tech. rep., SAE Technical Paper, 2006.
- [20] J. M. Levin, A. A. Paranjape, and M. Nahon, "Agile maneuvering with a small fixed-wing unmanned aerial vehicle," *Robotics and Autonomous Systems*, vol. 116, pp. 148–161, 2019.
- [21] H. Pacejka and I. Besselink, "Magic formula tyre model with transient properties," *Vehicle system dynamics*, vol. 27, no. S1, pp. 234–249, 1997.

- [22] J. H. Jeon, S. Karaman, and E. Frazzoli, "Anytime computation of time-optimal off-road vehicle maneuvers using the RRT," *Proceedings of the IEEE Conference on Decision and Control*, pp. 3276–3282, 2011.
- [23] Y. Lu, B. Yang, and Y. Mo, "Two-timescale mechanism-and-data-driven control for aggressive driving of autonomous cars," 2021.
- [24] A. Feddaoui, N. Boizot, E. Busvelle, and V. Hugel, "High-gain extended kalman filter for continuous-discrete systems with asynchronous measurements," *International Journal of Control*, vol. 93, no. 8, pp. 2001–2014, 2020.
- [25] I. Kasa, "A circle fitting procedure and its error analysis," *IEEE Transactions on Instrumentation and Measurement*, vol. IM-25, pp. 8–14, 1976.
- [26] C. Cao and N. Hovakimyan, "L1 adaptive output feedback controller to systems of unknown dimension," in *2007 American Control Conference*, pp. 1191–1196, 2007.
- [27] R. Hindman, C. Cao, and N. Hovakimyan, *Designing a High Performance, Stable L1 Adaptive Output Feedback Controller*.